Modulation of Drug Resistance in Ovarian Adenocarcinoma Using Chemotherapy Entrapped in Hyaluronan-Grafted Nanoparticle Clusters

Keren Cohen,[†,‡,§] Rafi Emmanuel,[†,‡,§] Einat Kisin-Finfer,[⊥] Doron Shabat,[⊥] and Dan Peer[†,‡,§,*]

[†]Laboratory of NanoMedicine, Department of Cell Research and Immunology, George S. Wise Faculty of Life Sciences, [‡]Department of Materials Sciences and Engineering, Faculty of Engineering, [§]Center for Nanoscience and Nanotechnology, and [⊥]School of Chemistry, Tel Aviv University, Tel Aviv 69978, Israel

ABSTRACT Resistance to anticancer drugs is considered a major cause of chemotherapy failure. One of the major mediators of resistance is the multidrug extrusion pump protein, P-glycoprotein (P-gp), an ATP-binding cassette (ABC) transporter with broad substrate specificity. In order to bypass this drug resistance mechanism, we have devised phospholipid-based nanoparticle clusters coated with the glycosaminoglycan hyaluronan, the major ligand of CD44, which is upregulated and undergoes different splice variations in many types of cancer cells. These particles, termed glycosaminoglycan particle nanoclusters or gagomers (GAGs), were self-assembled into ~500 nm diameter clusters, with zeta-potential values of ~−70 mV. Flow cytometry analysis provided evidence that, unlike free doxorubicin (DOX), a model chemotherapy, DOX entrapped in the GAGs (DOX-GAGs) accumulated in P-gp-overexpressing human ovarian adenocarcinoma cell line and dramatically decreased cell viability, while drug-free GAGs and the commercially available drug DOXIL (PEGylated liposomal DOX) did not produce therapeutic benefit. Furthermore, by using RNA interference strategy, we showed that DOX-GAGs were able to overcome the P-gp-mediated resistant mechanism of these cells. Most importantly, DOX-GAGs showed a superior therapeutic effect over free DOX in a resistant human ovarian adenocarcinoma mouse xenograft model. Taken together, these results demonstrated that GAGs might serve as an efficient platform for delivery of therapeutic payloads by bypassing P-gp-mediated multidrug resistance.

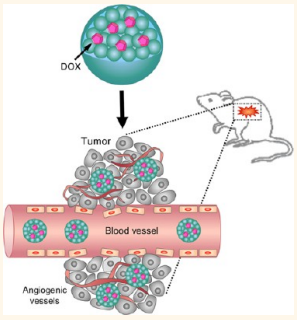

KEYWORDS: hyaluronan · cancer multidrug resistance · P-gp · lipid particle nanoclusters · doxorubicin

Multidrug resistance (MDR) is a major factor in the failure of many forms of chemotherapy in clinical oncology. As most chemotherapeutic agents have a low therapeutic index, even minimal changes in the sensitivity of tumor cells within patients can render their resistance. MDR can arise in numerous mechanisms, which can be noncellular or cellular-based. Noncellular mechanisms involve limited vascular accessibility and rapid clearance, which leads to inadequate intratumor drug concentration, or factors of the tumor cells' microenvironment, which inhibits damage-induced apoptotic signaling. Cellular mechanisms, which lead to MDR, involve enzymatic degradation, such as glutathione-S-transferase (GST), which leads to drug inactivation.[1,2] Yet, the main cellular-based mechanisms of MDR are the transport systems of the ATP-binding cassette (ABC) family. Overexpression of these transport proteins is responsible for drug resistance by pumping a variety of drugs out of the tumor cells at the expense of ATP hydrolysis.[2] The most studied and well-characterized ABC transporter is the multidrug transporter, P-glycoprotein (P-gp) or MDR1 protein, encoded by the *MDR1* gene.[3−5] In the clinic, the MDR phenotype is often associated with overexpression of the *MDR1* gene, which could be mediated by the exposure of the cancer cells to elevated levels of chemotherapeutic drugs.[6−12] The P-gp efflux pump has broad substrate specificity, which causes resistance for different drug families, such as anthracyclines, vinca alkaloids, podophyllotoxins, and taxanes, thus limiting their use in the clinic.[1,5] For example, in the case of doxorubicin (DOX), an anthracycline antibiotic commonly used in the treatment of hematopoietic and solid tumors,[13−15] resistant clones expressing high levels of P-gp often occur following the treatment especially in ovarian, colon,

* Address correspondence to peer@tauex.tau.ac.il.

Received for review October 3, 2013 and accepted February 4, 2014.

Published online February 04, 2014
10.1021/nn500205b

and breast carcinomas.[12,16−20] Higher doses of DOX cannot be administered due to undesirable adverse effects, mainly cardiotoxicity.[21,22] Two common strategies have long been used in order to overcome the resistance hurdles. First, many efforts have been made to find analogues of DOX with wider activity and lower toxicity. Yet, very few of these analogues become clinically useful, due to the fact that interrupting the original molecular structure of the drug usually resulted in a reduced anticancer activity and did not reduce the risk of cardiotoxicity.[23−25] The second strategy is using nanotechnology, such as the FDA-approved PEGylated liposomal formulation, named DOXIL.[26] DOXIL passively directs the drug into the tumor vicinity by exploiting the enhanced permeability and retention (EPR) effect and, thus, increases the local DOX concentration in the vicinity of the tumor. In addition, the PEG moiety also improves circulation time and stability of the drug carrier.[27] However, this formulation has a number of drawbacks, among them is the lack of active targeting abilities (ligand- or antibody-mediated) and complement activation.[28,29]

In order to take advantage of the DOX therapeutic effect on wide range of cancer cells while overcoming the MDR phenomenon and avoiding the significant toxicity associated with systemic administration of DOX, we have entrapped DOX in nanoparticulate carriers. These carriers include phospholipids that form lipid particle clusters, coated with the naturally occurring glycosaminoglycan, hyaluronan (HA), termed glycosaminoglycan particle nanoclusters, "GAGs".[30] We have previously reported that a similar particle, composed of the same components, was able to encapsulate the insoluble chemotherapy paclitaxel (PTX), which is a substrate of P-gp, as well, and efficiently deliver it to tumor cells in a syngeneic mouse model.[30] In this study, we have utilized these HA-coated lipid nanoparticle clusters to encapsulate a water-soluble drug (*i.e.*, DOX). HA is a water-soluble, nonimmunogenic polysaccharide. Since HA is the major ligand of CD44, which is expressed on almost all cell types, but is upregulated and undergoes different splice variations in cancerous cells, it can be exploited to actively target tumor cells.[31,32] We and others have demonstrated that HA can be covalently attached to lipid nanoparticles and efficiently target epithelial cancer cells and leukocytes expressing HA receptors.[22,30,33−37] In particular, we have managed to show that there was a clear increase in global affinity of HA to CD44 as a function of HA M_w, either free or particle-bound HA: high molecular weight HA (≥700 kDa) had a higher affinity toward CD44 than smaller HA fragments.[38] Moreover, HA endows the GAGs a hydrophilic coat, which promotes long circulation. Drug-loaded HA-coated lipid nanoparticles have been shown to increase drug accumulation in CD44-expressing tumors, decrease systemic toxicity, and increase survival time in multiple cancer models.[22,35]

Herein, we have chosen the human ovarian adenocarcinoma cell line NCI/ADR-Res (NAR) as our model system for MDR. In ovarian cancer, MDR is considered a major cause of chemotherapy failure and might be particularly involved in the secondary treatment failure frequently observed in the clinic.[1] NAR cells are multidrug-resistant, P-gp-expressing cells, derived by continuous exposure to increasing DOX concentrations in cell culture. We show that DOX-GAG particles are significantly more potent than the free drug in suppressing the growth and the proliferation of the highly resistant NAR cells. We were able to demonstrate that the DOX-GAGs internalize into the cells and overcome the efflux mechanism mediated by P-gp. Moreover, our *in vivo* results show that DOX-GAGs improve the therapeutic window of entrapped DOX relative to the free drug.

RESULTS AND DISCUSSION

GAG Surface Properties, Physicochemical, and Structural Analyses. The drug-free GAGs and DOX-GAGs have amorphous shapes as evidenced by TEM images (Figure 1A,B). The addition of DOX to the GAG preparation did not affect their size distribution and zeta-potential (Figure 1C). Mean hydrodynamic diameters were 447.7 ± 64.5 and 516.03 ± 76.3 nm for drug-free GAGs and DOX-GAGs, respectively, as determined by dynamic light scattering (DLS). The zeta-potential of empty GAGs was −77.5 ± 4.29 mV. Small, insignificant increase to −69.56 ± 4.59 mV was observed in the DOX-GAG formulation. This result is in contrast to our previously studied paclitaxel (PTX) -GAG nanoparticle clusters. In that study, we observed a significant increase in GAGs' hydrodynamic diameter when PTX was added.[30] PTX in contrast to DOX is a poorly water-soluble drug, which tends to incorporate inside the lipid layer of the particle, whereas DOX would be retained in the aqueous phase of the particle. Therefore, we argue that DOX utilizes the aqueous core and does not change the particle size distribution.

The zeta-potential of a nanoparticle is commonly used to characterize the surface charge property of nanoparticles.[39] It reflects the electrical potential of particles and is influenced by the composition of the particle and the medium in which it is dispersed. Increase in particle zeta-potential can enhance the electrostatic repulsive force, suppress the agglomeration, and subsequently reduce the dispersion and hydrodynamic diameter. Nanoparticles with a zeta-potential above ±30 mV have been shown to be stable in suspension, as the zeta layer prevents aggregation of the particles.[40−42]

DOX loading was at 1:12 drug/lipid (mol/mol). DOX release profile from the GAGs (Figure 2) was processed according to eq 1 and found to fit the case of two drug pools (*i.e.*, $n = 2$) with a rather fast dissipation of unencapsulated DOX and significantly slower efflux

A.

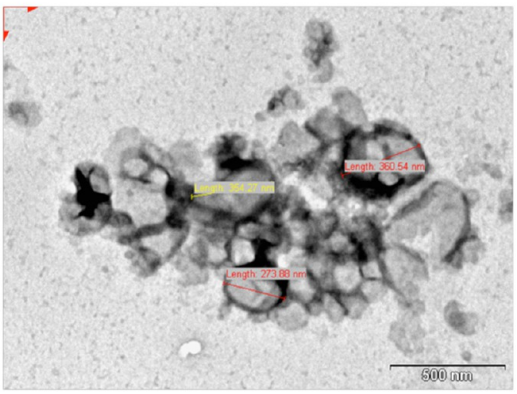

B.

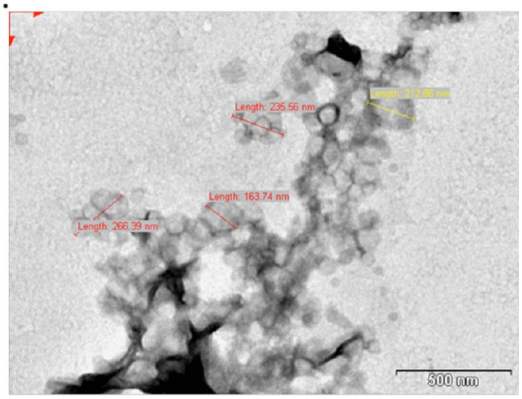

C.

Particles	Hydrodynamic Diameter (nm)	Zeta potential (mV)
Drug-free GAGs	447.7±64.5	-77.5±4.3
DOX-GAGs	516±76.3	-69.6±4.6

Figure 1. DOX-GAG structural and physicochemical properties. Representative images of the ultrastructure of (A) drug-free GAGs and (B) DOX-GAGs using TEM show the amorphous shape of the particles. (C) Hydrodynamic diameters and zeta-potential measurements of drug-free GAGs and DOX-GAG particle clusters. Data are expressed as the mean ± SD of at least three independent measurements.

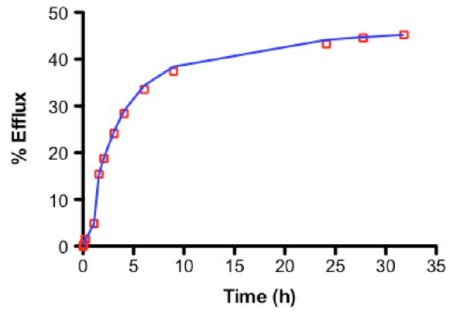

Figure 2. DOX release profile from GAGs. The points are experimental, each an average of duplicates, and the solid curves are the theoretical expectations; the results are of data analysis according to eq 1 (see Methods for more details) for the case of $n = 2$.

of the encapsulated drug. The rate constant determined for the efflux of encapsulated DOX from GAGs, 2.3×10^{-3} h^{-1}, corresponds to a half-life of 12 days. The DOX encapsulation efficiency was 60(±4)%.

GAGs Reduce DOX IC_{50} Values in Highly Resistant Cells. NAR cells were originally derived from OVCAR-8 cells that acquired DOX resistance due to high expression of P-gp following continuous exposure to increasing concentrations of the Adriamycin (DOX).[9] Figure 3 shows the expression levels of P-gp in (A) NAR and (B) OVCAR-8 cells.

In order to demonstrate the advantage of the encapsulated DOX *versus* the free DOX, we compared the IC_{50} values of DOX-GAG and the free DOX in the NAR cells with the parental OVCAR-8 cells (Figure 4). The cells were incubated for 4 h with equivalent concentrations of free or GAG-encapsulated DOX, then, cells were washed and incubated with drug-free media for additional 68 h. Cell viability was determined by XTT assay 72 h post-treatment termination. OVCAR-8 IC_{50} value of the free DOX was relatively low, with an IC_{50} value of ~1 μM, while poor cytotoxicity was obtained in the NAR cell line with an IC_{50} value of ~80 μM. The IC_{50} value of DOX-GAGs was similar to that of the free drug in OVCAR-8 cells (Figure 4A). This can be explained by faster accumulation of the free DOX in this sensitive cell line. The free drug passively diffuses into the cells, with no other barrier than the cell membrane. In contrast, when DOX-GAGs were applied onto the NAR-resistant cells (Figure 4B), they showed a superior cytotoxicity, with at least 8-fold lower IC_{50} values compared to the free drug, ~10 μM. In addition, we compared side-by-side commercially available PEGylated liposomal doxorubicin (DOXIL) with free DOX and DOX-GAGs (Figure 4B). DOXIL did not release its DOX payload during the incubation period, and thus, IC_{50} values could not be determined. Similar trend was observed in OVCAR-8 cells when DOXIL was used (data not shown).

We suggest that GAGs protect DOX from being effluxed by P-gp pumps that are expressed on NAR cells. This helps more drug molecules to enter and be retained in the resistant cells. This DOX cellular retention translates into more potent cytotoxicity.

Next, we wanted to test if the GAGs induce adverse immune activation when interacting with leukocytes. We previously showed that HA-coated lipid-based nanoparticles do not activate the complement system or induce cytokines in T cells.[38] Herein, we examined the protein secretion of the pro-inflammatory cytokine TNF-α, the general inflammatory cytokine IL-6, and the anti-inflammatory cytokine IL-10, which reciprocally regulate TNF-α secretion in RAW264.7 murine macrophage cell line.[43] LPS was used as a positive control

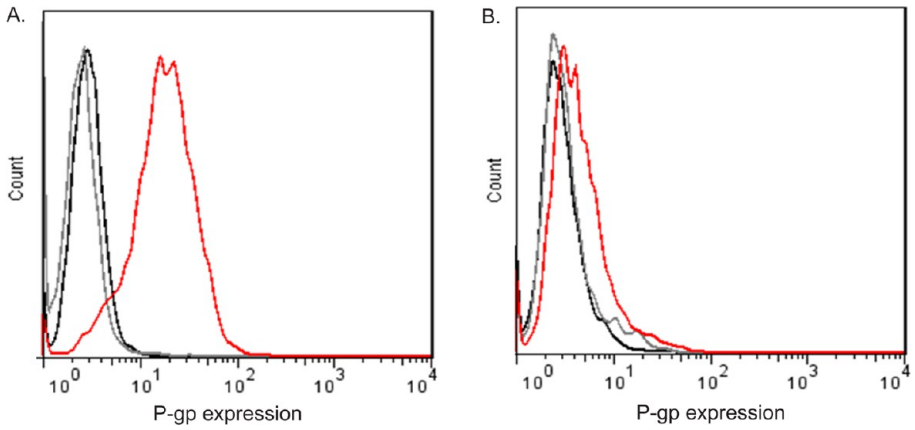

Figure 3. P-gp expression in NAR and OVCAR-8 cells. Representative histograms of P-gp expression in (A) NAR and (B) OVCAR-8 cells determined by flow cytometry. Black line, no stain; gray line, isotype control; red line, anti-P-gp.

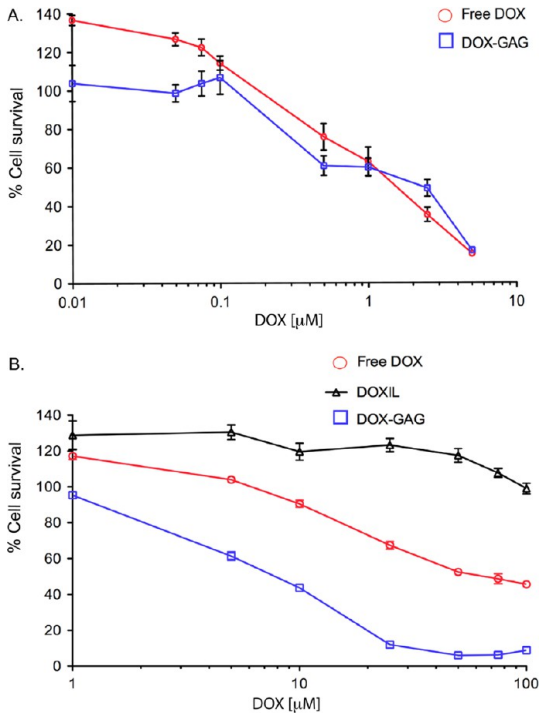

Figure 4. GAGs reduce DOX IC_{50} values in highly resistant cells: (A) OVCAR-8 and (B) NAR cell viability after 4 h treatment with free DOX, DOXIL, and DOX-GAGs. Cell viability was measured 72 h post-treatment termination by normalizing the viability of the treated cells to the mock treated cells and to the drug-free GAG-treated cells. Normal cell growth and viability were unaffected by drug-free GAGs in all the doses tested. Data are expressed as the mean ± SD of at least three independent experiments.

activating TLR4 and generating a pro-inflammatory response[44] (see Methods section and Supplementary Figure 1 in Supporting Information). We have not observed any triggering on these cytokines during the exposure of the GAGs to the cells (Supplementary Figure 1).

GAGs Loaded with DOX Overcome the P-gp Resistance Mechanism in NAR Cells. According to our hypothesis, the accumulation of the encapsulated drug in the cells is not affected by the expression level of P-gp. To ratify our assumption, we examined the effect of P-gp knockdown on the accumulation of free and encapsulated DOX in NAR cells. NAR cells were transfected with specific siRNA against P-gp (siP-gp) and against luciferase (siLuc) in order to exclude off-target silencing effects. Seventy-two hours post-transfection, cells treated with non-endogenous siLuc control showed similar P-gp levels to that of mock untransfected cells, thus no significant off-target silencing effect was observed. Cells treated with siP-gp showed 70% reduction in P-gp expression levels compared to the siLuc (Figure 5A). These cells were treated with 10 μM free or equivalent amounts of DOX-GAGs for 4 h, then the cells were washed and fresh medium was added. The efflux rate of the drug was estimated by measuring the DOX signal in these cells by flow cytometry at several time intervals after the addition of the fresh medium. The portion of free DOX remaining in NAR cells treated with siP-gp or siLuc is depicted in Figure 5B; siLuc-treated cells, which express high levels of P-gp protein, lost the majority (~50%) of the drug already 0.5 h after the end of the treatment. DOX efflux continued until steady state was achieved 4 h after the end of the treatment. As expected, siP-gp-treated cells, which express lower levels of P-gp efflux pumps, lost only ~25% of DOX after 0.5 h compared to siLuc-treated cells. In addition, the efflux rate of the drugs from these cells was slower. On the other hand, the efflux rate of the encapsulated drug was the same in both siP-gp-treated and siLuc-treated cells (Figure 5C). This result supports the hypothesis that GAGs protect DOX from being extruded from the cells by P-gp efflux pumps and enables the drug to sufficiently accumulate in the resistant cells compared to the free drug.

GAGs Loaded with DOX Bind to NAR Cells. Next, we examined the binding of GAGs-DOX to NAR surface using E-SEM analysis. NAR cells exhibit microvilli-like structures on the cell surface, as seen in Figure 6A and in a close up in Figure 6B. An impressive attachment of GAG-DOX onto NAR cells was observed already at

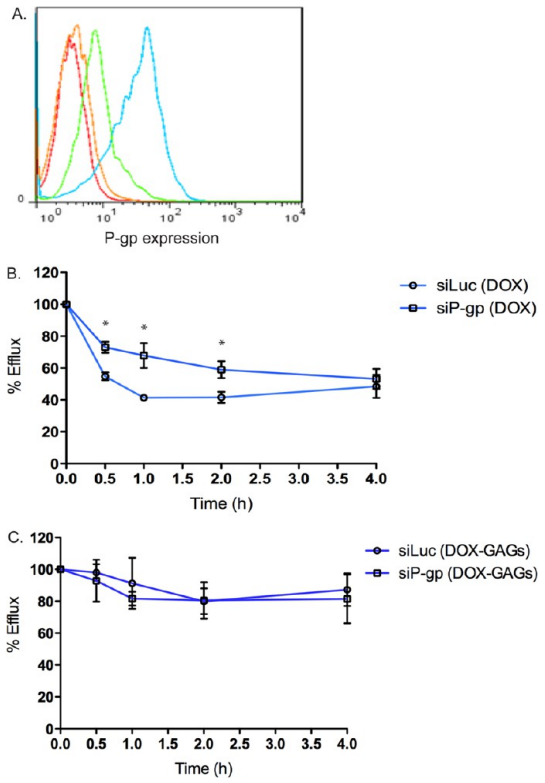

Figure 5. DOX-loaded GAGs shift the balance between influx and efflux of DOX. (A) Representative histograms of P-gp expression in NAR cells after downregulation of P-gp with siP-gp. Red line, no stain; orange line, isotype control; green line, siP-gp-treated cells; blue line, siLuc-treated cells. The percentage of DOX remaining in siLuc and siP-gp-treated NAR cells upon treatment with (B) free DOX and (C) DOX-GAGs; ∗ denotes $p < 0.05$.

30 min post-incubation (Figure 6C and in a close up in Figure 6D) with mean particle diameter of ~200 nm. This discrepancy in size distribution is attributed to the particular method used. DLS measurements in solution always increase the particle diameter especially for HA-coated particles that tend to adsorb water molecules,[38] whereas the use of EM always decreases the particle diameter after dehydration.

GAGs Internalized into NAR Cells. To examine the ability of GAGs to bind with high affinity to NAR cells and be internalized into the cells, we performed a confocal analysis as detailed in the Methods section. Internalization of DOX-GAGs into NAR cells occurred within 30 min post-incubation (Figure 7, 0.5 h) and more enhanced fluorescent signal after 4 h (Figure 7, 4 h). We confirmed that indeed DOX-GAGs are within the cells by confocal analysis (Figure 7, z-stack). This observation may suggest that GAGs prevent the drug molecules from being in close proximity to the P-gp pumps, and unlike the free DOX, DOX-GAGs are not rapidly effluxed from the cells and accumulate in the cells to reach cytotoxic levels.

DOX-Loaded GAGs Improve the Therapeutic Effect in NAR Xenograft Mouse Model. In order to study the efficacy of the DOX-GAGs *in vivo*, we established a human xenograft mouse model of NAR cells. NAR cells, stably expressing EGFP, were subcutaneously injected above the right femoral joint of female nude mice. The tumor dimensions were monitored by the EGFP fluorescence expressed by the cells using Maestro live imaging system (Figure 8A,B) and by caliper measurements, as well. In order to investigate the compatibility of the solid tumor model for particles' drug delivery, we examined the presence of paraneoplastic blood vessels in tumors 14 days post-tumor inoculation. Representative H&E staining of tumor sections are shown in Figure 8. These sections show viable tumors, without necrosis (C). A larger magnification shows the presence of many blood vessels (D).

DOX, like many other chemotherapeutic agents, is rapidly metabolized and eliminated by the reticuloendothelial system (RES) as fast as several minutes.[26] DOX encapsulation in GAGs, coated with the long-circulating agent HA, contributes to steric stabilization of the vesicles and provides protection from opsonization. This may eventually increase the therapeutic index of the drug by reducing the frequency and the amount of drug administered into patients, the adverse effects, and fluctuation in circulating drug levels.[22,35] We examined the pharmacokinetics of DOX-GAGs in nude mice bearing a NAR tumor examining both the retention in circulation and in the tissues of the GAGs (using Cy5-labeled GAGs) and the DOX amounts in the circulation and in selected tissues (including the tumor). The mice (n = 5/group) were injected with Cy5-labeled DOX-GAGs at 5 mg/kg DOX 14 days post cell inoculation. The pharmacokinetics of Cy5-labeled DOX-GAGs was assayed at several time points after intravenous (i.v.) administration. Most of the Cy5 signal was picked in the organs 5 h post-injection (Figure 9A) and from the blood 1 h post-injection (Figure 9B). Free DOX is eliminated from the circulation within several minutes (Figure 10A). This observation is in good agreement with several studies reported in the past.[22] DOX-GAGs were long circulating, and a substantial amount of DOX was still detected in the plasma of mice 72 h post-administration. $AUC_{0-\infty}$ of DOX was 6 and 836 (μg/mL × h) for free DOX and DOX-GAGs, respectively. This long-circulation property of the drug is attributed to the hydrophilic coating provided by HA, which endows these carriers with long-circulation properties.

We next tested the amount of DOX in different tissues at a designated time point of 24 h post-i.v. injection (Figure 10B): 23.5 ± 2.33% of DOX injected dose/gram tissue accumulated in the tumors when delivered *via* the GAGs compared with 0.45 ± 0.12% of DOX when free DOX was administered (Figure 10B). In addition, reduction in DOX accumulation in the liver and spleen was observed when DOX was delivered *via* GAGs (Figure 10B). These data were nicely correlated with the retention of Cy5-labeled DOX-GAGs in the tumor vicinity that lasted up to 24 h post-injection,

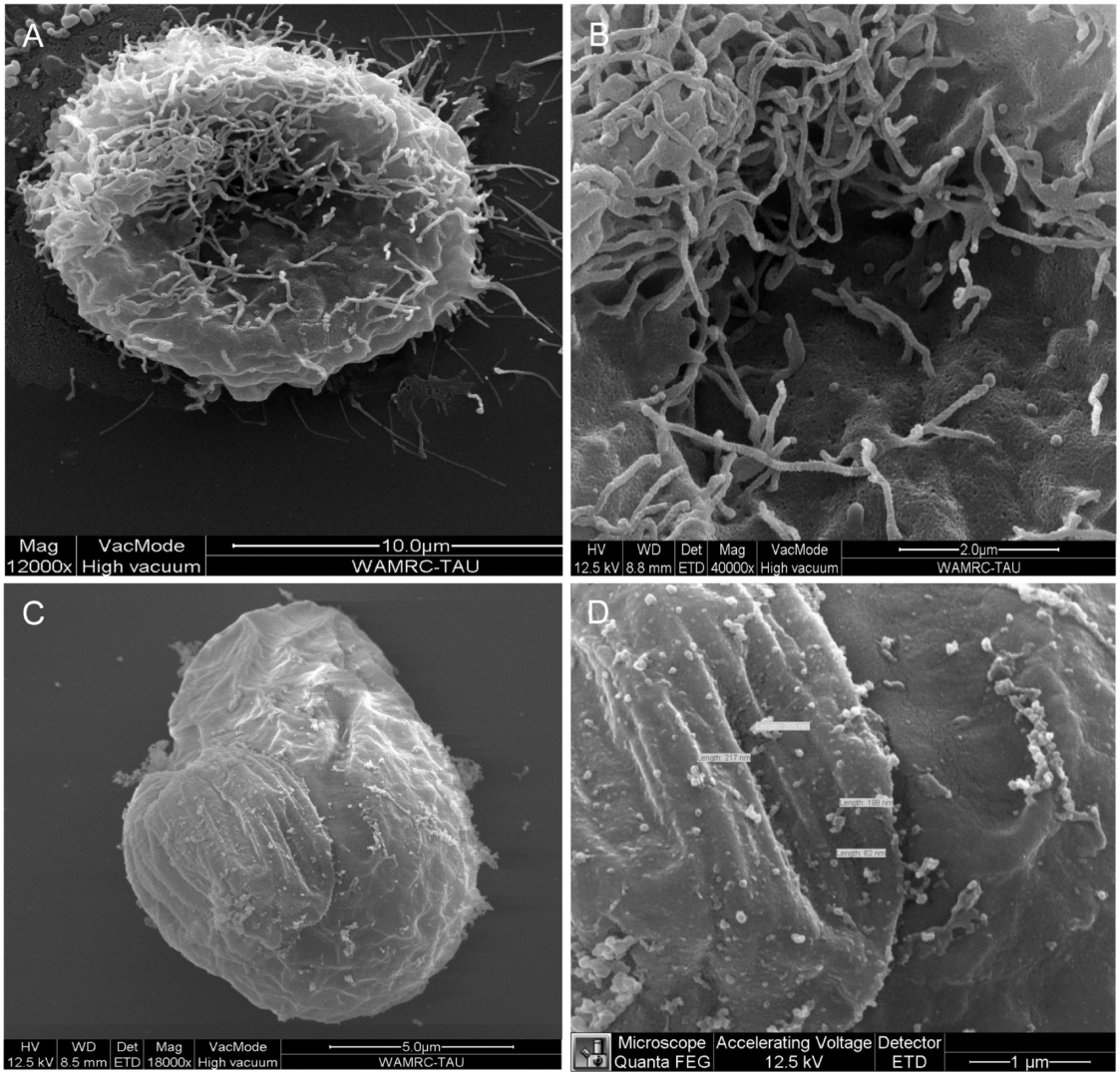

Figure 6. NAR cells surface morphology visualized by scanning electron micrograph (SEM). Cells were incubated either with growth media (mock-treated) (A) or with DOX-GAGs (C) for 30 min. Subsequently, cells underwent a prefixation treatment for visualization by SEM. Mock-treated NAR cells showed numerous microvilli-like structures, while treated cells changed their morphology and showed smooth surface with numerous lumps, which are the GAG clusters. (B,D) Higher magnification of (A) and (C), respectively.

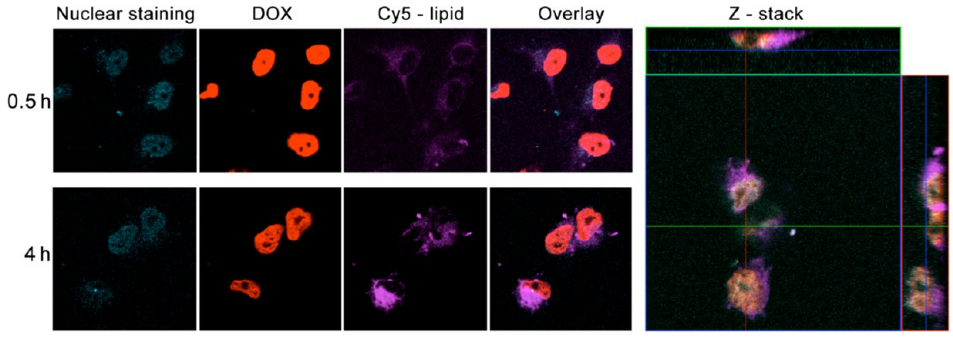

Figure 7. DOX-GAGs internalize into NAR cells. Confocal microscopy analysis of NAR cells after treatment with DOX-GAGs (including z-stack): NAR cells were incubated with Cy5-labeled DOX-GAGs. At indicated time points, cells were washed and fixed with 4% PFA. Nuclear staining was visualized using Hoechst 33342. The confocal images indicate enhancement of the DOX-GAG internalization in a time-dependent manner. The z-stack images were taken at 4 h post-incubation. The three-dimensional cutout shows that Cy5-labeled GAGs are localized at the cytosolic portion of the cells while DOX has already escaped the GAGs and entered the nucleus. Red and green lines indicate corresponding points in the orthogonal planes, showing localization of the label within the pictured cell. The images were taken with a Zeiss META confocal microscope using a 40× oil lens. The z-stack image was acquired with 10.3 μm stack size along the *z*-axis.

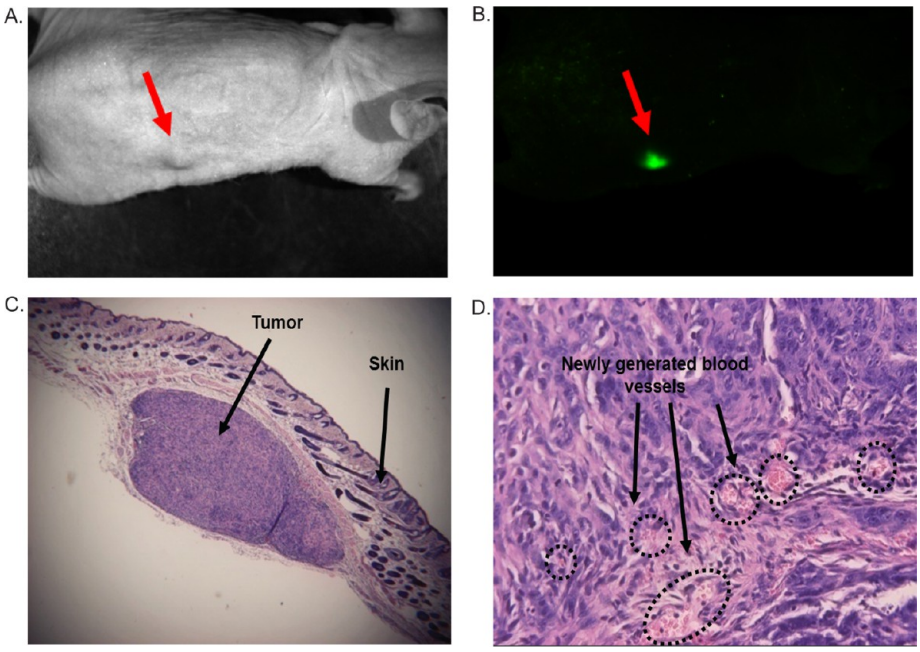

Figure 8. NAR tumor xenograft establishment. (A) Bright-field and (B) fluorescent images of nude mouse bearing a tumor of EGFP-expressing NAR cells. The arrowhead indicates the tumor area. (C) Gross morphology of NAR tumors after H&E staining showing viable tumor tissue without any significant necrosis areas, magnification 4×. (D) Microscopic morphology of NAR tumor reveals distinct vascular pattern with tumor cell aggregated around the blood vessels (black dashed cycles), magnification 20×.

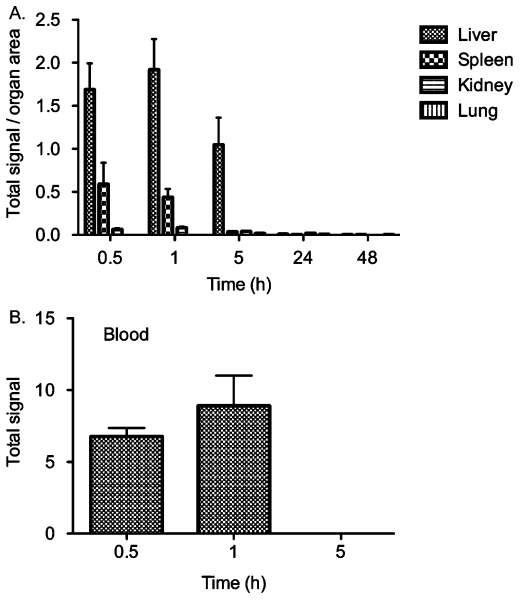

Figure 9. Pharmacokinetics and tissue distribution of Cy5-GAGs in NAR xenograft model. Biodistribution of Cy5-labeled GAGs loaded with DOX in different organs (A) and in the blood (B). Detection of Cy5-GAGs in the organs was assayed by the Maestro *in vivo* fluorescence imaging system (CRi MA, USA). Calculation of total signal/organ area of Cy5 *versus* time after injection was performed using the Maestro software.

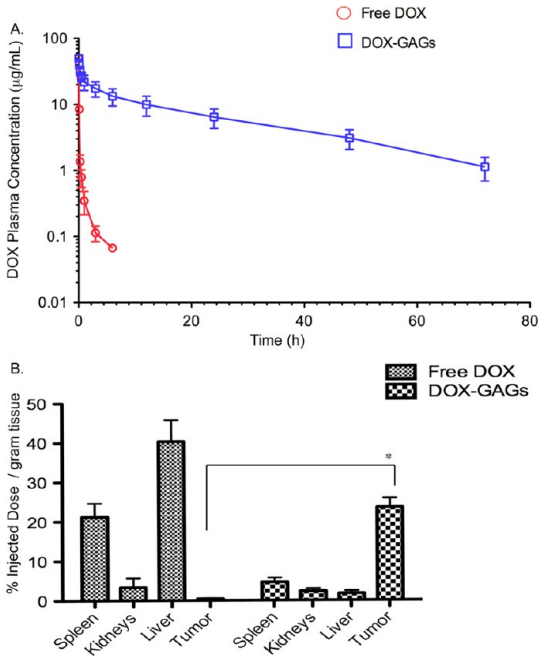

Figure 10. Pharmacokinetics and tissue distribution of DOX-GAGs in NAR xenograft model. Biodistribution of GAGs loaded with DOX in the plasma (A) and in different organs (including tumors) (B). Detection of DOX in the organs was assayed by using fluorescence as listed in the Methods section; ∗ indicates a *P* value of 0.000183.

as estimated by confocal microscopy analysis of sliced tumor sections (Figure 11A).

In order to study the therapeutic effect of DOX-GAGs in comparison to the free DOX *in vivo*, mice with tumors obtained 14 days post-tumor inoculation were intravenously administered with either HBSS (mock-treated), drug-free GAGs, 2 mg/kg DOX, or 1 mg/kg DOX-GAGs, three times a week for 4 weeks (Figure 11B). The size of the tumors was monitored using Maestro live

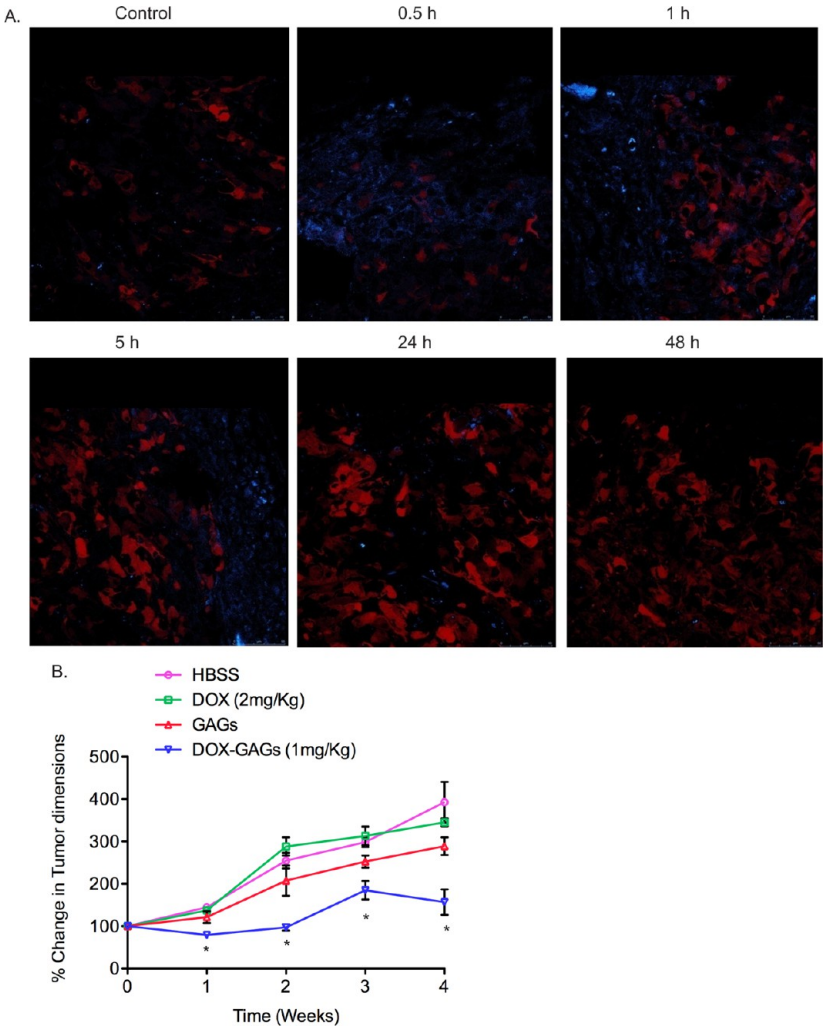

Figure 11. Retention of Cy5-labeled DOX-GAGs and therapeutic effect in human NAR xenograft. Retention of Cy5-labeled DOX-GAGs in the tumor vicinity after a single i.v. injection into human NAR xenograft model. Analysis of cryo-sectioned tumors was done using confocal microscopy (A). Red, NAR tumor cells; blue, Cy5-labeled DOX-GAGs. (B) Therapeutic efficacy was demonstrated using i.v. injections every other day post-initiation of the experiment with doses and formulations as listed. Data are expressed as the mean ± SEM of (n = 5/group); * P < 0.01.

imaging system. The encapsulated drug significantly attenuated the growth of the tumors relative to the free drug and the control treatments without any observed clinical toxicity (Figure 11B). It has been previously reported that perturbing the interaction of HA with its receptors reduce tumor formation, in mice bearing melanoma tumors established from CD44-expressing tumor cell lines.[45,46] The moderate reduction in tumor dimensions in mice treated with drug-free GAGs might be explained by this phenomenon. An exogenous HA, which is bound to the GAGs, might compete with the endogenous natural ligands, which exist in the tumor microenvironment, and as a result interferes with the interaction between tumor cells and host tissue stroma, a critical event in tumor growth and metastasis.

The transport of particles inside the tumor is governed by many factors, among them physiological (high interstitial pressure) and physiochemical properties (composition, structure, charge) of the tumor and physiochemical properties of the particle (size, geometry, charge, hydrophobicity).[47] Optimization of some of the particles' physiochemical properties, such as size and surface properties, might influence the *in vivo* fate of nanoparticles. Surface hydrophobicity of nanoparticles determines the amount of adsorbed blood components, mainly proteins (opsonins). This in turn influences the *in vivo* fate of nanoparticles.[48,49] Binding of these opsonins onto the surface of nanoparticles will eventually lead to opsonization of these particles, mainly by the reticuloendothelial system (RES), and they could be trapped in sinusoidal barriers such as in the liver, spleen, and lungs. Hence, to increase the likelihood of the success in drug targeting by nanoparticles, it is necessary to minimize the opsonization and to prolong the circulation time of nanoparticles *in vivo*. In order to achieve this goal, GAGs coated with a hydrophilic polymer, HA, which in addition to its role in targeting endows the GAGs a hydrophilic coat that creates a cloud of chains at the

particle surface, which may repel plasma proteins. In addition to the charged face of HA, due to the carboxylic groups of the glucuronic acid, it also has a hydrophobic face, which is contributed by the clusters of hydrogen atoms. HA molecules are able to adsorb to one another *via* hydrophobic interactions.[50] It is well-established that particle diameter is an important factor that determines their *in vivo* fate. Usually, particles ranging from 10 to 500 nm in diameter can extravasate and accumulate inside the interstitial space of the tumor due to the increased vascular permeability, depending on the "cut-off" size of the permeabilized vasculature, which can vary from person to person and from tumor to tumor.[47] As described earlier, the hydrodynamic diameter of GAGs was in the upper limit of this range. Thus, reduction of the GAGs' diameter might improve their retention in the tumor vicinity and increase their tumor penetration.[51] In addition, we have previously shown that ~100 nm diameter liposomes coating the HA at M_w > 700 kDa have higher affinity to the HA receptor, CD44, as evident by very low K_d values,[38] thus we strongly believe that GAG reduction in diameter may facilitate not only tumor penetration but also higher therapeutic effect.

CONCLUSIONS

Our results indicate that the DOX-GAG formulation was able to bypass the P-gp-mediated drug resistance pumps. As a result, GAGs managed to increase the influx/efflux ratio of DOX inside the cancerous cells and were found to be superior to the free DOX both *in vitro* and *in vivo*. In addition, we demonstrated that the commercially available PEGylated liposomal doxorubicin (DOXIL) that is often used to treat resistant ovarian tumors in the clinic did not affect NAR cells viability while DOX-GAGs decrease dramatically the cell viability and caused cell death.

DOX-GAGs retained at the vicinity of the tumors 24 h post-i.v. administration while cleared from other organs within 5 h following i.v. administration. This observation was also confirmed when DOX was extracted from the tumors and from different organs, demonstrating a robust tumor accumulation (~23% of ID/gram tissue) when delivered *via* GAGs compared with ~0.5% of ID/gram tissue for free DOX. This differential uptake by the tumor cells could be explained by utilizing both the passive (EPR effect) and the active CD44-HA-mediated targeting, which increased the amount of DOX in the tumor and thus increased the therapeutic effect *in vivo*.

In this study, the DOX represents a water-soluble molecule and was formulated in the GAGs, which were initially developed as nanovectors for insoluble drugs (*e.g.*, PTX). We suggest that these vehicles might be suitable for carrying both soluble and insoluble drugs simultaneously. As a result of different machineries in cancer cells, GAGs could be used to achieve more efficient treatment and ultimately might become a new therapeutic modality in treating highly resistant tumors in the clinic.

METHODS

Preparation of Drug-Free and DOX-Loaded GAGs. Lipids 1,2-dilauroyl-*sn*-glycero-3-phosphoethanolamine (DLPE) and 1,2-dilauroyl-*sn*-glycero-3-phosphoglycerol (DLPG) (Avanti Polar Lipids, Inc., AL, USA) at a mole ratio of 9:1, respectively, were mixed and dissolved in ethanol. The solution was evaporated to dryness under reduced pressure in a Buchi rotary evaporator vacuum system (Flawil, Switzerland) and hydrated by the swelling solution that consisted of MES buffer (0.1 M, pH 5.5) with or without DOX (drug loading was 1:12 drug/lipid (mol/mol)). Prior to the addition of activated HA (at weight ratio of total lipid/HA 10:1 (w/w)), the suspension was heated at 60 °C for 2 h. HA (Lifecore Biomedical, LLC (MN, USA)) at a M_w of 700 kDa was dissolved in MES buffer (0.1 M, pH 5.5) to final concentration of 2 mg/mL and preactivated by incubation with sulfo-NHS (Proteochem) and EDAC (Sigma-Aldrich Co., St. Louis, MO, USA) for 15 min at room temperature. The cross-linking reaction was most efficient at molar ratio of 1:2:2 (COOH/s-NHS/EDAC). The activated HA was added to the lipid suspension and incubated overnight, at room temperature. Excess reactive agents and byproducts were removed by three cycles of ultracentrifugation (Sorval, ThermoFisher, Waltham, MA, USA) at 386 000*g*, 45 min each cycle. In the first cycle, the MES buffer was replaced with HEPES buffer saline (HBS) (20 mM HEPES, 150 mM NaCl) pH 8.2, and in the last two cycles, the buffer was HBS at pH 7.4. GAGs were sonicated for 10 min in a bath sonicator, lyophilized, and kept at −20 °C until further use. Prior to an experiment, GAGs were resuspended in the cell growth medium to the same prelyophilization volume and sonicated for 10 min using a bath sonicator. In order to determine DOX quantity in the DOX-GAG batches, the lipids were disassembled by treatment with 1% deoxycholate at 37 °C for 1 h, and DOX fluorescence was measured.

Cy5-DLPE Conjugate Synthesis. Cy5-NHS was synthesized according to previously published experimental procedure.[52] Cy5-NHS (54 mg, 0.086 mmol) was dissolved in 2 mL of DMF and 1 mL of $CHCl_3$. Then DLPE (50 mg, 0.086 mmol) was added followed by the addition of Et_3N (18 μL, 0.129 mmol). The reaction mixture was heated to 50 °C and stirred ON. The reaction was monitored by RP-HPLC (grade 10−90% ACN in H_2O, 20 min). Upon completion, the solvent was removed under reduced pressure and the crude product was purified by column chromatography on silica gel (3:7 MeOH/DCM) to afford Cy5-DLPE conjugate (58 mg, 64%) as a blue solid (Scheme 1). ^{1}H NMR (400 MHz, $CDCl_3$): δ = 8.41 (1H, m), 7.82 (2H, dt, J = 12.9, 5.1 Hz), 7.40−7.35 (4H, m), 7.27−7.19 (4H, m), 7.10 (1H, d, J = 7.9 Hz), 6.81 (1H, t, J = 13.9 Hz), 6.42 (1H, d, J = 13.7 Hz), 6.31 (1H, d, J = 13.4 Hz), 5.23 (1H, m), 4.43 (1H, dd, J = 12.1, 2.5 Hz), 4.22−4.17 (1H, m), 4.10−4.07 (4H, m), 4.05−4.03 (4H, m), 3.46 (2H, m), 2.30−2.25 (6H, m), 1.81 (2H, m), 1.78−1.74 (2H, m), 1.70 (12H, s), 1.56−1.52 (4H, m), 1.44−1.37 (2H, m), 1.25 (32H, m), 0.89−0.85 (9H, m). HPLC grade 10−90% ACN in water 20 min, retention time = 19.8 min, λ = 640 nm. See NMR spectrum in Supplementary Figure 2A−D.

Particle Size Distribution and Zeta Potential Measurements. The hydrodynamic size and surface charge (zeta-potential) of GAGs were characterized using the ZetaSizer Nano ZS (Malvern Instruments Inc., UK), utilizing dynamic light scattering (DLS) and electrophoretic light scattering (ELS), respectively.[53] Each experimental result is an average of at least three independent measurements.

Ultrastructure Analysis. The ultrastrcture of GAGs and DOX-GAGs was investigated using transmission electron microscope

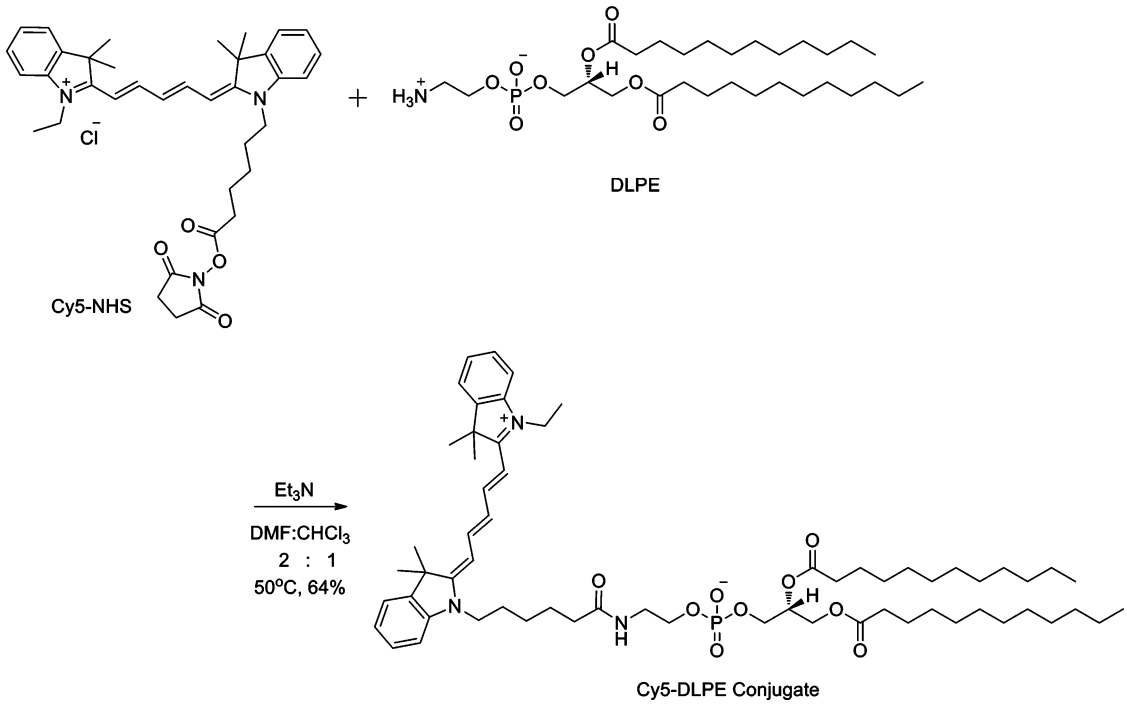

Scheme 1. Chemical synthesis of the Cy5-DLPE conjugate.

(TEM). Samples were adsorbed on Formvar/carbon-coated grids and negatively stained with 2% aqueous uranyl acetate. Samples were examined using Jeol 1200EX TEM (Jeol, Japan).

Drug Efflux and Encapsulation Efficiency. The kinetics of drug efflux was studied as previously described.[54−56] Briefly, a suspension of GAGs (0.5−1.0 mL) was placed in a dialysis sac, and the sac was immersed in a continuously stirred receiver vessel, containing drug-free buffer (HBS at pH 7.4). The buffer volume in the receiver vessel was 10- to 16-fold higher than that of the GAG sample in the dialysis sac. At designated periods, the dialysis sac was transferred from one receiver vessel to another, containing fresh (*i.e.*, drug free) buffer. Drug concentration was assayed in each dialysate and in the sac (at the beginning and end of each experiment). In order to obtain a quantitative evaluation of drug release, experimental data were analyzed according to a previously derived multipool kinetic model,[55,56] in which drug efflux from the sac into the reservoir occurs from a series of independent drug pools, one corresponding to free (*i.e.*, unencapsulated) drug and all others to GAG-associated drug. The overall drug release corresponds to the following equation:

$$f(t) = \sum_{j=1}^{n} f_j(1 - \exp^{-k_j t}) \quad (1)$$

where t denotes time, $f(t)$ is the cumulative drug released into the dialysate at time t, normalized to the total drug in the system at time 0, f_j is the fraction of the total drug in the system occupying the jth pool at time = 0, and k_j is the rate constant for drug diffusion from the jth pool.

The data analysis of efflux kinetics is also used to calculate the encapsulation efficiency. As discussed above, magnitudes of the parameter f_j are obtained through data analysis. When the efflux experiment is carried out on samples from the complete GAG preparation, the sum of f_j(s) for the pool(s) of encapsulated drug is also the efficiency of encapsulation.

Quantitative Determinations of DOX. DOX was assayed by its fluorescence. The measurement was determined with Synergy HT multi-mode microplate reader (BioTek. VT, USA) with an excitation at 490 nm and emission maximum at 560−590 nm using a standard curve.

Tumor Cell Lines and Cell Culture. Monolayers of NCI/ADR-RES (NAR) (P-gp-overexpressing human ovarian adenocarcinoma DOX-resistant), OVCAR-8 (DOX-sensitive cell line), and RAW264.7 (mouse macrophages) cells were grown in 100 × 20 mm dishes. NAR and OVCAR-8 cells were cultured in RPMI-1640. RAW264.7 cells were cultured in Dulbecco's modified Eagle's medium (DMEM). All growth media contained 10% fetal bovine serum, penicillin (100 U/mL), streptomycin (0.1 mg/mL), nystatin (12.5 U/mL), and L-glutamine (2 mM). Cells were free of mycoplasma contamination as determined by a mycoplasma PCR test carried out every 3 months. Viability of cultures used in the experiments was >90%, as determined by the trypan blue method.

Preparation of EGFP-Expressing NAR Cells. NAR cells were stably transfected with 3 μg of pEGFP-N1 vector (Clontech) using Lipofectamine 2000 transfection reagent (invitrogen). The cells were positively selected using 0.5 mg/mL G418 24 h after the transfection. The transfected cells were sorted according to their GFP expression, and the highest GFP population was collected.

Flow Cytometry Analysis. Cells of each kind were incubated with either mouse IGg2a isotype control (BioLegend, San Diego, CA, USA) or mouse monoclonal anti-human P-gp (clone 4E3), which recognizes an external epitope of the protein (ABCAM, Cambridge, MA, USA), on ice for 30 min. After being washed, samples were incubated with a fluorescein isothiocyanate (FITC)-labeled goat polyclonal secondary antibody to mouse IgG antibody (ABCAM, Cambridge, MA, USA) for 30 min at 4 °C in the dark. Samples were centrifuged and resuspended in PBS containing 1% FCS for analysis on a Becton Dickinson FACScalibur flow cytometer with CellQuest software (Becton Dickinson, Franklin Lakes, NJ). Ten thousand events were determined for each test sample. Excitation was by a single 15mW argon-ion laser beam (488 nm). Emission was collected through a 530 nm band-pass filter. Data analysis was performed using FlowJo software (Tree Star, Inc., OR, USA).

***In Vitro* Cytotoxicity Studies.** NAR and OVCAR-8 cells were seeded into 96-well plates at 2.5 × 10^3 and 7 × 10^3 cells/well, respectively, and allowed to attach overnight. Cells were incubated for 4 h with equivalent concentrations of free, GAG-encapsulated DOX, or commercial DOXIL (PEGylated liposomal doxorubicin). Cell proliferation was determined by XTT assay 72 h after the termination of the treatment, and IC_{50} values were calculated based on the percentage of treatment over control.

Cytokine Induction Assay. RAW264.7 cells were seeded 24 h prior to the experiment in 96-well plate at a density of 7.5 × 10^4

cells per well. The cells were incubated with the selected treatment media containing DOX, drug-free GAGs, and DOX-GAGs for 6 h. Cell stimulation with 100 ng/mL LPS was used as positive control. The levels of TNF-α, IL-10, and IL-6 secreted to the medium were measured by DuoSet ELISA Development kits (R&D systems, Minneapolis, MN, USA).

Silencing P-gp with siRNA. For P-gp silencing experiments, NAR cells were seeded in 6-well plates at a density of 7.5×10^4 per well. After 24 h, the cells were transfected with siRNA targeting *MDR-1* gene encodes P-gp (siP-gp) (Dharmacon Research, Inc.) using oligofectamine and OPTI-MEM I reduced serum medium (Life Technologies, Inc., Carlsbad, CA), according to the manufacturer's protocol. NAR cells were also transfected with siRNAs, which is directed against the non-endogenous gene, luciferase, in addition to mock-transfected control cells, which were treated with serum-reduced medium. The final concentration of siRNA was 25 nM. The changes in P-gp surface protein expression were measured by flow cytometry 72 h after the transfection using the flow cytometry analysis detailed above.

Quantification of Free or Encapsulated DOX in NAR Cells. Seventy-two hours post-transfection, siP-gp- and siLuc-treated NAR cells were incubated for 4 h with 10 μM of free or encapsulated DOX. After the termination of the treatment, cells were washed and detached from the plate and DOX fluorescence was measured by a Becton Dickinson FACScalibur flow cytometer (CA, USA) at several time points: 0, 0.5, 1, 2, 4 h after the treatment. Ten thousand events were determined for each test sample. Excitation was by a single 15 mW argon-ion laser beam (488 nm). Emission was collected through a 585 nm band-pass filter. Data analysis was performed using FlowJo software (Tree Star, Inc., OR, USA).

Cell Surface Analysis Using Scanning Electron Microscopy. NAR cells (3×10^4) were seeded on cover slides and allowed to attach overnight. Cells were incubated for 30 min with DOX-GAGs containing 10 μM DOX. At the end of the treatment, samples were washed with PBS and fixed in 2.5% glutaraldehyde in PBS. After being washed, the samples were dehydrated by successive ethanol treatment. After critical point drying (Balzer's critical point drier), the samples were mounted on aluminum stubs and sputter-coated (E5100, Polaron) with gold. The samples were investigated in high vacuum mode Quanta 200 FEG ESEM.

Confocal Microscopy Analysis. NAR cells were seeded on cover slides and allowed to attach overnight. Cells were incubated for 4 h with Cy5-labeled DOX-GAGs containing 10 μM DOX. At the end of the treatment, cells were subjected to three washes with PBS and fixed with 4% paraformaldehyde (PFA) solution. Then, cells were stained with Hoechst 33342 (Sigma-Aldrich) nucleic acid staining. The cells were subjected to three washes with PBS and were fixed with mounting medium. Confocal images were acquired with a Zeiss META confocal microscope (Zeiss, Jena, Germany).

NAR Xenograft Model. Athymic nude female mice (6 weeks old) were purchased from Harlan Laboratories (Israel). Mice were maintained and treated according to National Institutes of Health guidelines. All animal protocols were approved by the Tel-Aviv Institutional Animal Care and Use Committee. Mice were implanted with 2×10^6 NAR-GFP cells in 0.2 mL of Hanks' balanced salt solution (HBSS) (Bet Ha'emek, Israel) subcutaneously just above the right femoral joint. Fourteen and 21 days after tumor inoculation, mice were sacrificed and tumors were removed, postfixed in 4% PFA in PBS pH 7.4 overnight in room temperature, and subjected to hematoxylin and eosin (H&E) staining.

Pharmacokinetics and Tissue Distribution. The experiment was performed 14 days post-tumor inoculation. Each mouse was administered by a single intravenous injection of Cy5-labeled DOX-GAGs (5 mg/kg body weight of DOX). After the formulation administration, the mice were randomly separated into five groups (n = 3/group). Each group was sacrificed in a defined time period after the formulation administration (0.5, 1, 5, 24, 48 h). Blood samples were collected by submandibular bleeding method. The blood samples were immediately mixed with 25 μL of 0.5 mM EDTA-PBS, followed by a 5 min centrifugation at 200*g*; the supernatant was collected, and Cy5 was assayed using the Maestro *in vivo* fluorescence imaging system (CRi MA, USA). Calculation of total signal of Cy5 *versus* time after injection was performed using the Maestro software (CRi MA, USA). After the blood withdrawal, the mice were anesthetized and sacrificed. Liver, spleen, kidneys, lungs, and tumors were removed immediately. Detection of Cy5-GAGs in the organs was assayed by the Maestro *in vivo* fluorescence imaging system (CRi MA, USA). Calculation of total signal/organ area of Cy5 *versus* time after injection was performed using the Maestro software. Tumors were fixed in 4% PFA in PBS pH 7.4 overnight in room temperature protected from light. Next, the tumors were cryoprotected in sucrose gradient (10% sucrose for 2 h, 20% for 2 h, 30% overnight) in 4 °C protected from light. Finally, the tumors were transferred into OCT for embedding overnight in 4 °C protected from light, and each tumor was sectioned by Leica 3050 S cryomicrotome (Leica Microsystems, Wetzlar, Germany). Confocal images of GFP-expressing tumor cells and Cy5-labeled DOX-GAGs were acquired on a Leica TC SP5 II STED with spatial resolution of 50−70 nm (Leica, Wetzlar, Germany).

Pharmacokinetics of the Drug (DOX) Component. The experiment was performed 14 days post-tumor inoculation. Each mouse was administered by a single intravenous injection of DOX-GAGs (5 mg/kg body weight of DOX). After the formulation administration, the mice were randomly separated into 2 groups (n = 7/group). Each group was sacrificed in a defined time period after the formulation administration up to 72 h. Blood samples were collected by submandibular bleeding method and assayed as previously described.[22] The blood samples were immediately mixed with 250 μL of 0.5 mM EDTA-PBS, followed by a 5 min centrifugation at 200*g*. DOX was assayed in both cell and supernatant fractions as follows: the pelleted cells and the supernatant from the first centrifugation were separated, and the cells were subjected to a wash (including recentrifugation) in the EDTA-PBS solution. The supernatants from both runs were combined and assayed for DOX. DOX was extracted from the cells by incubation with 2.5 mL of acidic isopropyl alcohol (81 mM HCl in isopropyl alcohol) for 4 h at 4 °C, followed by centrifugation under the same conditions specified above. The supernatants, containing the extracted DOX, were also subjected to assay and found to contain negligible amounts of DOX (<0.001% of injected dose). Calculation of area under the curve (AUC) of concentration *versus* time was performed using the WinNonLin 4.0.1 program (Pharsight Corporation, Mountain View, CA) by a Non-Compartment model 201 (intravenous bolus administration).

Tissue Distribution of DOX. Each group was divided into two subgroups (n = 7 per subgroup), receiving a single intravenous dose of a selected formulation on day 14 from tumor inoculation. Treatment groups included free DOX and DOX-GAGs. DOX dose in all injected mice was 5 mg/kg body, and details of administration are as listed above for pharmacokinetics. Twenty-four hours post-injection, the mice were anesthetized and sacrificed. Liver, spleen, kidneys, lungs, and NAR tumors were removed immediately after perfusion with saline, and each organ was weighed and examined by a pathologist blinded to the experimental groups. Each organ was then homogenized; DOX was extracted as described above for pharmacokinetics and assayed.

Therapeutic Efficacy Studies. Treatments were initiated 14 days post-tumor inoculation when tumor volumes reached ~15 mm^3 (day 0). Tumor volume was calculated as $(\text{width})^2 \times \text{length}/2$. The mice were randomly separated into four groups (n = 6/group): (1) HBSS, (2) free DOX, (3) DOX-GAGs, and (4) empty GAGs. The doses in the free DOX and in the DOX-GAG formulations were 2 and 1 mg/kg body, respectively, and treatments were given every 48 h according to the results of the pharmacokinetics and tissue distribution studies. Administration was by intravenous injection of 100 μL of the selected formulation to the lateral tail vein, using a 27-gauge needle. Tumor dimensions were assayed by GFP fluorescence using the Maestro *in vivo* fluorescence imaging system (CRi MA, USA). Calculation of average signal/counts per seconds of GFP was performed using the Maestro software (CRi MA, USA). Values of change in tumor dimensions were calculated based on the percentage over tumor dimensions on day 0.

Statistics. Differences between two means were tested using an unpaired, two-sided Student's t-test. Differences between treatment groups were evaluated by one-way ANOVA test of SPSS software.

Conflict of Interest: The authors declare the following competing financial interest(s): D.P. has a financial interest in Quiet Therapeutics.

Acknowledgment. This work was supported in part by the grants from the Lewis Family Trust, the Israeli Centre of Research Excellence (I-CORE), Gene Regulation in Complex Human Disease, Center No 41/11; FTA: Nanomedicine for Personalized Theranostics, and by The Leona M. and Harry B. Helmsley Nanotechnology Research Fund awarded to D.P.

Supporting Information Available: Cytokine induction in macrophages by DOX, drug-free GAGs, and DOX-GAGs and NMR spectrum of Cy5-DLPE. This material is available free of charge *via* the Internet at http://pubs.acs.org.

REFERENCES AND NOTES

1. Agarwal, R.; Kaye, S. B. Ovarian Cancer: Strategies for Overcoming Resistance to Chemotherapy. *Nat. Rev. Cancer* **2003**, *3*, 502–516.
2. Ullah, M. F. Cancer Multidrug Resistance (MDR): A Major Impediment to Effective Chemotherapy. *Asian Pac. J. Cancer Prev.* **2008**, *9*, 1–6.
3. Ambudkar, S. V.; Lelong, I. H.; Zhang, J.; Cardarelli, C. O.; Gottesman, M. M.; Pastan, I. Partial Purification and Reconstitution of the Human Multidrug-Resistance Pump: Characterization of the Drug-Stimulatable ATP Hydrolysis. *Proc. Natl. Acad. Sci. U.S.A.* **1992**, *89*, 8472–8476.
4. Chen, C. J.; Chin, J. E.; Ueda, K.; Clark, D. P.; Pastan, I.; Gottesman, M. M.; Roninson, I. B. Internal Duplication and Homology with Bacterial Transport Proteins in the Mdr1 (P-Glycoprotein) Gene from Multidrug-Resistant Human Cells. *Cell* **1986**, *47*, 381–389.
5. Gottesman, M. M.; Pastan, I. Biochemistry of Multidrug Resistance Mediated by the Multidrug Transporter. *Annu. Rev. Biochem.* **1993**, *62*, 385–427.
6. Choi, C. H. ABC Transporters as Multidrug Resistance Mechanisms and the Development of Chemosensitizers for Their Reversal. *Cancer Cell Int.* **2005**, *5*, 1–13.
7. Hille, S.; Rein, D. T.; Riffelmann, M.; Neumann, R.; Sartorius, J.; Pfützner, A.; Kurbacher, C. M.; Schöndorf, T.; Breidenbach, M. Anticancer Drugs Induce Mdr1 Gene Expression in Recurrent Ovarian Cancer. *Anticancer Drugs* **2006**, *17*, 1041–1044.
8. Hotta, T.; Tanimura, H.; Tsunoda, T.; Iwahashi, M.; Tani, M.; Noguchi, K.; Mizobata, S.; Arii, K.; Terasawa, H.; Nakamori, M.; *et al.* P-Glycoprotein Expression and Chemosensitivity in Highly Purified Fresh Human Gastrointestinal Cancer Cells. *Hepatogastroenterology* **1999**, *46*, 316–321.
9. Liscovitch, M.; Ravid, D. A Case Study in Misidentification of Cancer Cell Lines: MCF-7/Adrr Cells (Re-Designated NCI/ADR-RES) Are Derived from OVCAR-8 Human Ovarian Carcinoma Cells. *Cancer Lett.* **2007**, *245*, 350–352.
10. Schondorf, T.; Neumann, R.; Benz, C.; Becker, M.; Riffelmann, M.; Göhring, U. J.; Sartorius, J.; von König, C. H.; Breidenbach, M.; Valter, M. M.; *et al.* Cisplatin, Doxorubicin and Paclitaxel Induce Mdr1 Gene Transcription in Ovarian Cancer Cell Lines. *Recent Results Cancer Res.* **2003**, *161*, 111–116.
11. Tokunaga, Y.; Hosogi, H.; Hoppou, T.; Nakagami, M.; Tokuka, A.; Ohsumi, K. Effects of MDR1/P-Glycoprotein Expression on Prognosis in Advanced Colorectal Cancer after Surgery. *Oncol. Rep.* **2001**, *8*, 815–819.
12. Yu, S. T.; Chen, T. M.; Tseng, S. Y.; Chen, Y. H. Tryptanthrin Inhibits MDR1 and Reverses Doxorubicin Resistance in Breast Cancer Cells. *Biochem. Biophys. Res. Commun.* **2007**, *358*, 79–84.
13. Apetoh, L.; Mignot, G.; Panaretakis, T.; Kroemer, G.; Zitvogel, L. Immunogenicity of Anthracyclines: Moving towards More Personalized Medicine. *Trends Mol. Med.* **2008**, *14*, 141–151.
14. Dal Ben, D.; Palumbo, M.; Zagotto, G.; Capranico, G.; Moro, S. DNA Topoisomerase II Structures and Anthracycline Activity: Insights Into Ternary Complex Formation. *Curr. Pharm. Des.* **2007**, *13*, 2766–2780.
15. Hande, K. R. Topoisomerase II Inhibitors. *Cancer Chemother. Biol. Response Modif.* **2003**, *21*, 103–125.
16. Linn, S. C.; Giaccone, G. MDR1/P-Glycoprotein Expression in Colorectal Cancer. *Eur. J. Cancer* **1995**, *31*, 1291–1294.
17. Peer, D.; Dekel, Y.; Melikhov, D.; Margalit, R. Fluoxetine Inhibits Multidrug Resistance Extrusion Pumps and Enhances Responses to Chemotherapy in Syngeneic and in Human Xenograft Mouse tumor models. *Cancer Res.* **2004**, *64*, 7562–7569.
18. Schondorf, T.; Kurbacher, C. M.; Gohring, U. J.; Benz, C.; Becker, M.; Sartorius, J.; Kolhagen, H.; Mallman, P.; Neumann, R. Induction of MDR1-Gene Expression by Antineoplastic Agents in Ovarian Cancer Cell Lines. *Anticancer Res.* **2002**, *22*, 2199–2203.
19. Shen, D. W.; Fojo, A.; Chin, J. E.; Roninson, I. B.; Richert, N.; Pastan, I.; Gottesman, M. M. Human Multidrug-Resistant Cell Lines: Increased Mdr1 Expression Can Precede Gene Amplification. *Science* **1986**, *232*, 643–645.
20. Toole, B. P.; Slomiany, M. G. Hyaluronan, CD44 and Emmprin: Partners in Cancer Cell Chemoresistance. *Drug Resist. Updates* **2008**, *11*, 110–121.
21. Gabizon, A. A. Liposomal Drug Carrier Systems in Cancer Chemotherapy: Current Status and Future Prospects. *J. Drug Target* **2002**, *10*, 535–538.
22. Peer, D.; Margalit, R. Tumor-Targeted Hyaluronan Nanoliposomes Increase the Antitumor Activity of Liposomal Doxorubicin in Syngeneic and Human Xenograft Mouse Tumor Models. *Neoplasia* **2004**, *6*, 343–353.
23. Arcamone, F. Properties of Antitumor Anthracyclines and New Developments in Their Application: Cain Memorial Award Lecture. *Cancer Res.* **1985**, *45*, 5995–5999.
24. Minotti, G.; Menna, P.; Salvatorelli, E.; Cairo, G.; Gianni, L. Anthracyclines: Molecular Advances and Pharmacologic Developments in Antitumor Activity and Cardiotoxicity. *Pharmacol. Rev.* **2004**, *56*, 185–229.
25. Monneret, C. Recent Developments in the Field of Antitumour Anthracyclines. *Eur. J. Med. Chem.* **2001**, *36*, 483–493.
26. Gabizon, A.; Catane, R.; Uziely, B.; Kaufman, B.; Safra, T.; Cohen, R.; Martin, F.; Huang, A.; Barenholz, Y. Prolonged Circulation Time and Enhanced Accumulation in Malignant Exudates of Doxorubicin Encapsulated in Polyethylene-Glycol Coated Liposomes. *Cancer Res.* **1994**, *54*, 987–992.
27. Allen, T. M.; Cullis, P. R. Drug Delivery Systems: Entering the Mainstream. *Science* **2004**, *303*, 1818–1822.
28. Chanan-Khan, A.; Szebeni, J.; Savay, S.; Liebes, L.; Rafique, N. M.; Alving, C. R.; Muggia, F. M. Complement Activation Following First Exposure to PEGylated Liposomal Doxorubicin (Doxil): Possible Role in Hypersensitivity Reactions. *Ann. Oncol.* **2003**, *14*, 1430–1437.
29. Moghimi, S. M.; Hamad, I.; Andresen, T. L.; Jorgensen, K.; Szebeni, J. Methylation of the Phosphate Oxygen Moiety of Phospholipid-Methoxy(polyethylene glycol) Conjugate Prevents PEGylated Liposome-Mediated Complement Activation and Anaphylatoxin Production. *FASEB J.* **2006**, *20*, 2591–2593.
30. Rivkin, I.; Cohen, K.; Koffler, J.; Melikhov, D.; Peer, D.; Margalit, R. Paclitaxel-Clusters Coated with Hyaluronan as Selective Tumor-Targeted Nanovectors. *Biomaterials* **2010**, *31*, 7106–7114.
31. Mizrahy, S.; Peer, D. Polysaccharides as Building Blocks for Nanotherapeutics. *Chem. Soc. Rev.* **2012**, *41*, 2623–2640.
32. Peer, D. A Daunting Task: Manipulating Leukocyte Function with RNAi. *Immunol. Rev.* **2013**, *253*, 185–197.
33. Eliaz, R. E.; Nir, S.; Szoka, F. C., Jr. Interactions of Hyaluronan-Targeted Liposomes with Cultured Cells: Modeling of Binding and Endocytosis. *Methods Enzymol.* **2004**, *387*, 16–33.
34. Eliaz, R. E.; Szoka, F. C., Jr. Liposome-Encapsulated Doxorubicin Targeted to CD44: A Strategy To Kill CD44-Overexpressing Tumor Cells. *Cancer Res.* **2001**, *61*, 2592–2601.
35. Peer, D.; Margalit, R. Loading Mitomycin C Inside Long Circulating Hyaluronan Targeted Nano-liposomes Increases Its Antitumor Activity in Three Mice Tumor Models. *Int. J. Cancer* **2004**, *108*, 780–789.
36. Peer, D.; Park, E. J.; Morishita, Y.; Carman, C. V.; Shimaoka, M. Systemic Leukocyte-Directed SiRNA Delivery Revealing Cyclin D1 as an Anti-inflammatory Target. *Science* **2008**, *319*, 627–630.
37. Platt, V. M.; Szoka, F. C., Jr. Anticancer Therapeutics: Targeting Macromolecules and Nanocarriers to Hyaluronan or CD44, a Hyaluronan Receptor. *Mol. Pharmaceutics* **2008**, *5*, 474–486.

38. Mizrahy, S.; Raz, S. R.; Hasgaard, M.; Liu, H.; Soffer-Tsur, N.; Cohen, K.; Dvash, R.; Landsman-Milo, D.; Bremer, M. G.; Moghimi, S. M.; *et al.* Hyaluronan-Coated Nanoparticles: The Influence of the Molecular Weight on CD44-Hyaluronan Interactions and on the Immune Response. *J. Controlled Release* **2011**, *156*, 231–238.
39. Couvreur, P.; Barratt, G.; Fattal, E.; Legrand, P.; Vauthier, C. Nanocapsule Technology: A Review. *Crit. Rev. Ther. Drug Carrier Syst.* **2002**, *19*, 99–134.
40. Araujo, F. A.; Kelmann, R. G.; Araujo, B. V.; Finatto, R. B.; Teixeira, H. F.; Koester, L. S. Development and Characterization of Parenteral Nanoemulsions Containing Thalidomide. *Eur. J. Pharm. Sci.* **2011**, *42*, 238–245.
41. Herran, E.; Perez-Gonzalez, R.; Igartua, M.; Pedraz, J. L.; Carro, E.; Hernandez, R. M. VEGF-Releasing Biodegradable Nanospheres Administered by Craniotomy: A Novel Therapeutic Approach in the APP/Ps1 Mouse Model of Alzheimer's Disease. *J. Controlled Release* **2013**, *170*, 111–119.
42. Woitiski, C. B.; Neufeld, R. J.; Ribeiro, A. J.; Veiga, F. Colloidal Carrier Integrating Biomaterials for Oral Insulin Delivery: Influence of Component Formulation on Physicochemical and Biological Parameters. *Acta Biomater.* **2009**, *5*, 2475–2484.
43. Goldsmith, M.; Avni, D.; Levy-Rimler, G.; Mashiach, R.; Ernst, O.; Levi, M.; Webb, B.; Meijler, M. M.; Gray, N. S.; Rosen, H.; *et al.* A Ceramide-1-Phosphate Analogue, PCERA-1, Simultaneously Suppresses Tumour Necrosis Factor-Alpha and Induces Interleukin-10 Production in Activated Macrophages. *Immunology* **2009**, *127*, 103–115.
44. Kedmi, R.; Ben-Arie, N.; Peer, D. The Systemic Toxicity of Positively Charged Lipid Nanoparticles and the Role of Toll-like Receptor 4 in Immune Activation. *Biomaterials* **2010**, *31*, 6867–6875.
45. Bartolazzi, A.; Peach, R.; Aruffo, A.; Stamenkovic, I. Interaction between CD44 and Hyaluronate Is Directly Implicated in the Regulation of Tumor Development. *J. Exp. Med.* **1994**, *180*, 53–66.
46. Zeng, C.; Toole, B. P.; Kinney, S. D.; Kuo, J. W.; Stamenkovic, I. Inhibition of Tumor Growth *in Vivo* by Hyaluronan Oligomers. *Int. J. Cancer* **1998**, *77*, 396–340.
47. Elinav, E.; Peer, D. Harnessing Nanomedicine for Mucosal Theranostics: A Silver Bullet at Last? *ACS Nano* **2013**, *7*, 2883–2890.
48. Brigger, I.; Dubernet, C.; Couvreur, P. Nanoparticles in Cancer Therapy and Diagnosis. *Adv. Drug Delivery Rev.* **2002**, *54*, 631–651.
49. Muller, R. H.; Wallis, K. H. Surface Modification of I.V. Injectable Biodegradable Nanoparticles with Poloxamer Polymers and Poloxamine 908. *Int. J. Pharm.* **1993**, *89*, 25–31.
50. Toole, B. P. Hyaluronan: From Extracellular Glue to Pericellular Cue. *Nat. Rev. Cancer* **2004**, *4*, 528–539.
51. Chauhan, V. P.; Stylianopoulos, T.; Martin, J. D.; Popović, Z.; Chen, O.; Kamoun, W. S.; Bawendi, M. G.; Fukumura, D.; Jain, R. K. Normalization of Tumour Blood Vessels Improves the Delivery of Nanomedicines in a Size-Dependent Manner. *Nat. Nanotechnol.* **2012**, *7*, 383–388.
52. Jung, M. E.; Kim, W. J. Practical Syntheses of Dyes for Difference Gel Electrophoresis. *Bioorg. Med. Chem.* **2006**, *14*, 92–97.
53. Delgado, A. V.; Gonzalez-Caballero, F.; Hunter, R. J.; Koopal, L. K.; Lyklema, J. Measurement and Interpretation of Electrokinetic Phenomena. *J. Colloid Interface Sci.* **2007**, *309*, 194–224.
54. Margalit, R.; Alon, R.; Linenberg, M.; Rubin, I.; Rosenman, T. J.; Wood, R. W. Liposomal Drug Delivery—Thermodynamic and Chemical Kinetic Considerations. *J. Controlled Release* **1991**, *17*, 285–296.
55. Margalit, R.; Okon, M.; Yerushalmi, N.; Avidor, E. Bioadhesive Liposomes for Topical Drug Delivery: Molecular and Cellular Studies. *J. Controlled Release* **1992**, *19*, 275–288.
56. Peer, D.; Margalit, R. Physicochemical Evaluation of a Stability-Driven Approach to Drug Entrapment in Regular and in Surface-Modified Liposomes. *Arch. Biochem. Biophys.* **2000**, *383*, 185–190.